On numerical investigation of heat transfer augmentation of flat target surface under impingement of steady air jet for varying heat flux boundary condition

Mohammed Umair Siddique[1,*], Ashfaq Syed[2], Sher Afghan Khan[3], Josua P. Meyer[1]

[1]Department of Mechanical and Aeronautical Engineering, University of Pretoria, Pretoria, South Africa

[2]Department of Automobile Engineering, M. H. Saboo Siddik College of Engineering, Mumbai, India

[3]Department of Mechanical Engineering, International Islamic University of Malaysia, Selangor, Malaysia

*Correspondence to Mohammed Umair Siddique. Email: Siddique.umair@up.ac.za

Abstract

The prediction of flow pattern for the proposed range of Reynolds number and nozzle–target spacing is carried out using SST + Gamma–Theta turbulence model. The simulations of the flow field in a computational domain are carried out using CFX as a base solver with 10^{-6} being the converging criteria. The present work aims to determine the local Nusselt number magnitude for varying heat flux input boundary conditions. Not only this, the impinging Reynolds numbers and nozzle–target spacing are also varied to record sufficient data, enough to predict a semi-empirical correlation. The proposed correlation for calculating the cooling characteristic (Nusselt number magnitude) under the impingement of air jet is presented in terms of profile heat flux parameter, impinging Reynolds number, and target to nozzle exit spacing. The corresponding mathematical parameter representing the profile heat flux boundary condition is the slope in heat flux magnitude versus the target surface's radial distance. The Nusselt number profile, which describes the cooling characteristic under different impinging Reynolds numbers and nozzle–target spacing, initially increases, takes a peek, and decreases. The rise in the cooling rate near the stagnation region is due to the turbulence palpitation, resulting from imbalance adverse pressure gradient and onset transition of Reynolds number. The local heat transfer under such boundary conditions increases with nozzle–target spacing and least depends on Reynolds number. However, the Nusselt profile for a constant heat flux magnitude but varying slope (non-uniform) shows an enhancement with a decrease in the slope from unit value.

Keywords

- Cooling rate
- Nusselt number
- Reynolds number
- Nozzle–target spacing
- Slope
- Varying heat flux

Abbreviations

L	Length of nozzle (Meters)
Z	Nozzle exit to target surface spacing (Meters)
x, r	Axial/ radial location (Meters)
GR	Growth rate
Q	Heat flux (Watts m^{-2})
ρ	Density of fluid (Kg m^{-3})
V	Velocity of fluid (M s^{-1})
g	Gravitation acceleration (M s^{-2})
f	Friction factor
Re	Reynolds number
Nu, Nu_0	Nusselt number
m	The slope of heat Flux
Z/d	Nozzle–target spacing
r/d	Non-dimensional radial location

Introduction

Cooling hot target surfaces such as heat sinks find an enormous research application in determining the cooling characteristics in many processing plants and microchips. In the last few years, the cooling of the heat sinks in many of these applications has found a jet impingement method. The cooling characteristic due to impingement is around 50 times higher than the traditional way of cooling by fans or blowers. Many high computational servers have now been designed for cooling using air jet impingement. The quenching processes in material processing industries are now modernized through impingement technology. Since the 1980s, many academic and industrial researchers have taken the initiative in determining the cooling rate due to jet impingement. At present, lots of parameters responsible for producing higher cooling due to jet impingement are investigated. The most exciting thing is that all researchers came up with a conclusion of Nusselt number representing the cooling rate parameter, which is unique.

Literature overview and scope of present work

Pamadi and Belov [1] observed two prominent secondary peaks for the lower nozzle–target (Z/d) spacing. The first peak was concluded due to the transition in flow regime and the second due to non-uniform turbulence. The occurrence of non-uniform turbulence along the non-dimensional axial/ radial distance (r/d) of the target surface is due to the under-development of the incoming jet's potential core. For the impingement of a jet on a target surface, the occurrence of a stagnation region, transition region, and uniform flow development is likely to be observed for a fully developed potential core (Katti and Prabhu [2]). Shadlesky [3] reported the importance of jet impingement point for an underdeveloped potential core in the area of ignition process for a rocket motor. No doubt, the stagnation point heat transfer is drastically affected due to the radial velocity gradient. Still, it is also affected due to the adverse pressure gradient, says Siddique et al. [4]. Jambunathan et al. [5]

did a massive review in this area. They reported the dependency of the Reynolds number and non-dimensional target to the nozzle exit spacing (Z/d) up to the non-dimensional radial distance (r/d) of 5 and also reported the independency of Nusselt profile for $Z/d > 6$. Mohanty and Tawfek [6] gave the unique non-dimensional empirical correlation for Nusselt number in Reynolds number and nozzle–target spacing. However, this was valid for an overall Nusselt number magnitude. An exponent of 0.70 and –0.25 was proposed for Reynolds number and Z/d. A very similar experimental work was carried out by Alimohammadi et al. [7], for a wide range of turbulent Reynolds numbers (4000–36,000) and Z/d ranges between 2 and 8. The focus of the study was toward the validation of the experimental readings with the numerical methodology. The numerical analysis was done by Alimohammadi et al. [7]. It clearly reported the use of intermediate transition models with the shear stress transport (SST) model for accurately predicting the Nusselt profile far as jet impingement is concerned. The advantage of these two-transition models lies in accurately developing the flow field in the near-wall region due to high pressure difference and local transition of the velocity gradient. Alimohammadi [8] even came forward with a pulse jet boundary condition at the nozzle's exit and reported the augmentation of heat transfer compared to a steady jet. In alignment with the previous experimental work carried out by Sailor et al. [9], Alimohammadi [8] gave in-depth data for the local Nusselt number for different pulse jet impingement conditions. Sailor et al. [9] have clearly stated the augmentation of the pulse jet compared to the steady jet; however, the work was limited to the findings of the overall Nusselt number and not the local Nusselt number. The jet's impingement on the target surface generates a Nusselt number profile, which should be dependent upon the heating boundary condition of the heat sink. The sink's heating can be done either by providing uniform heat at the bottom of the sink or by circulating the steam and maintaining the target surface at a constant temperature. Still, the Nusselt profile differences due to these two types of boundary conditions remain as a gap. The work of Alimohammadi et al. [7], Alimohammadi et al. [10, Sagot et al. [11] was carried out with a constant wall temperature boundary condition. On the other hand, the work of Katti and Prabhu [2, Siddique et al. [12], and Ekkad and Kontrovitz [13] was carried out under constant heat flux boundary. Considering the temperature profile for a flow in a circular pipe for these two boundary conditions, the Nusselt number along the length would be linear for constant heat flux boundary conditions and parabolic for constant wall temperature, says Yunus A Cenjel [14]. A very close observation toward the Nusselt profile along the radial length for impingement of jet and the axial length for a pipe flow is very similar. No doubts the cooling characteristics and magnitudes may differ and would be a strong function of Reynolds number, says Zuckerman and Lior [15]. According to Katti and Prabhu [2, Umair and Gulhane [16] and Zuckerman and Lior [15], three correlations exist for predicting the local Nusselt number. It is not possible to have a single empirical relation for predicting the local cooling characteristic (Nusselt number) throughout the radial distance since the profile is non-uniform. Katti and Prabhu [2] have defined these empirical relations for stagnation region ($0 < r/d < 1$), transition field ($1 < r/d < 2.5$) and near-wall region (r/d > 2.5). Siddique et al. [12] concluded the velocity gradient remark in the near-wall field up to r/d=2.5. Behnia et al. [17] clearly stated the confinement of air jet on local stagnation point Nusselt number. The confinement achieved was surrounding the jet with an isothermal wall. An extreme increment in the overall Nusselt number was observed by confining the jet at low nozzle–target spacing. However, the article also reported the significant importance of the Gamma–Theta transition model (Alimohammadi et al. [7]) in FLUENT/ CFX for accurate Nusselt profile prediction. Undoubtedly, the surplus turbulence generation over the target surface for an impinging of jet should produce higher heat transfer. Still, Ekkad and Kontrovitz [13] reported the decrement in heat transfer in the presence of the dimpled target

surface. However, care should be taken over the number of dimples on target surface, for minimizing the bursting turbulence phenomenon of flow separation and reattachment, says Ekkad and Kontrovitz [13]. Zuckerman and Lior [15] gave a very clear justification for the occurrence of intermittency, onset transition of Reynolds number, and flow separations for an impinging jet over a target surface. However, this turbulence phenomenon gets boosted for the under developed potential core of impinging jet.

As seen from the literature study, extensive work is done to predict the Nusselt number of target surface (Heat sink) in terms of inlet velocity (Reynolds number) and target to the nozzle exit spacing (Z/d). The maximum work is carried out with constant heat flux boundary conditions, and few are also carried out under continual temperature boundary conditions. Generally, for cooling the hot target surface for high computational servers, the actual heat flux input to such surfaces is not uniform. Hence, pumping power to dissipate a particular amount of heat is calculated, assuming a constant heat flux boundary condition is higher, whereas in the actual case, the heat input is not uniform. It is evident that the input pumping power calculation done for extraction of heat in high computational servers, which is non-uniform, is always higher than that required.

Objective of the paper

While scanning the literature and progress of the work carried out in the field of jet impingement, a vital research gap can be seen in the optimization of input power (Impingement) considering the non-uniform heat flux boundary conditions. The current work aims to determine the correlations for variable slopes (m) of non-uniform heat flux parameters, considering the inlet velocity (pumping power) and nozzle–target spacing. The computations are carried out for investigating local Nusselt numbers under different impinging Reynolds numbers, nozzle–target spacing, and slope of non-uniform heat flux. The local Nusselt number is presented against the non-dimensional radial distance (r/d), which is known as the Nusselt profile. At the end of the article, the author concludes the correlation for local Nusselt number in Reynolds number, Z/d, r/d and slopes for non-uniform heat flux (m). For the varying heat flux boundary condition, heat transfer phenomena are no longer similar to constant heat flux boundary conditions. This can be seen from the proposed empirical relation for the Nusselt number in terms of nozzle–target spacing and Reynolds number. The enhancement observed in the Nusselt profile with a decrease in the m of heat flux boundary condition is due to the pressure/ impinging velocity spots that arise from the stagnation region's upper skin.

Computational methodology

The computational domain consists of a circular target surface of 50 mm diameter, as the Nusselt number variation with impingement of jet doesn't exist beyond $r/d > 2.5$ (Katti and Prabhu [2]). The nozzle diameter is chosen to be the same as that of Katti and Prabhu [2](16 mm) for the current domain. The nozzle–target spacing can be varied from $Z/d = 2$ to 8. As shown in Fig. 1, the domain is axis-symmetric along vertical axis. The two-dimensional sketch shown in is revolved about 3 degrees to make it a 3-D model and hence compatible to the CFX solver. No doubt, the 2-D geometric model shall also render the same results as the proposed model. However, the author would not like to take the chance with 2-D. The reader must take care that the positive x–co-ordinate and the radial distance (r) are the same co-ordinates. The nozzle length is kept around $10D$, which is enough for the development of the air jet, according to Yunus A Cenjel [14]. The bottom surface of the heat sink is given a

uniform wall heat flux of 15,000 Wm^{-2} to get a fair gradient in cooling characteristics (Alimohammadi et al. [7]). The ambient domain is extended up to the end of the target surface, with the sink's sidewalls being assigned an isothermal boundary condition. (Alimohammadi et al. [7]). After striking the target surface, the air jet's outflow is set to the solver's opening boundary condition. However, entrainment of atmospheric air entrains into the jet is of the least concern (Ricou and Spalding [18]). The current geometry is designed with the commercial pack of the design modeler of ANSYS 19.3.

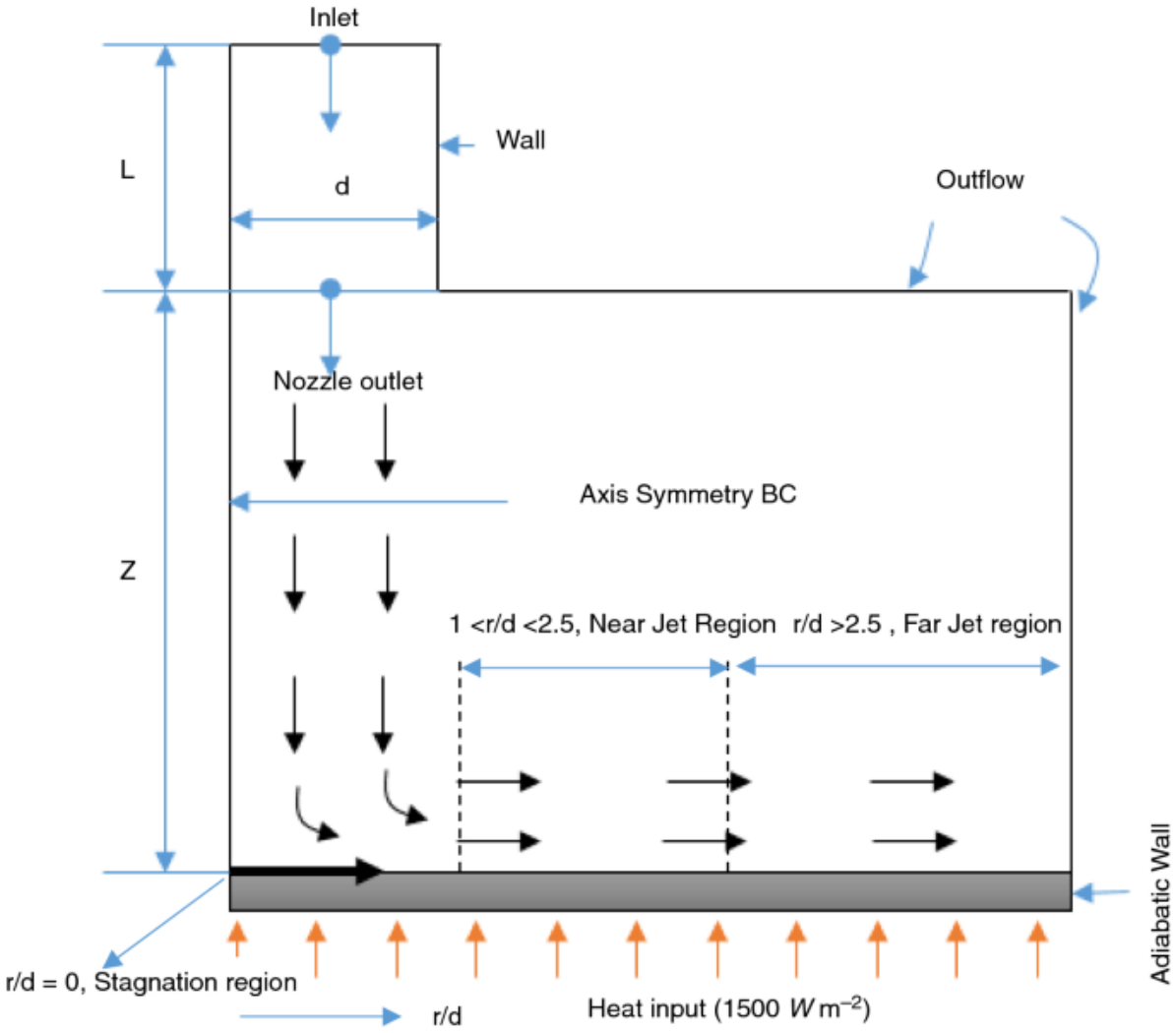

Fig. 1. Schematic sketch of the computational domain

Grid independence study

Meshing for the current domain is carried out within a commercial mesh modeler (ANSYS 19.3). Since the prediction of flow behavior in the ambient region expects the impinging jet region to be of the least use, the mesh density in this area is relatively coarse. Hexahedral mesh topology is adapted for the current domain (Alimohammadi et al. [10]). The target surface to nozzle outlet spacing (Z) and axial length of the target surface (r) are assigned 500

number of divisions (at least 10 unit cells per *mm* in a computational domain, says Siddique Mohd et al. [19]). The grid independence is achieved by varying the growth rate (*Z* and *r*). The growth rate for these two edges is varied from 1.2 to 1.025. As shown in Fig. 2, the Nusselt profiles for the mesh with growth rates of 1.05 and 1.025 coincide. Hence, the use of mesh topology with a growth rate of 1.025 should ensure an entirely accurate result.

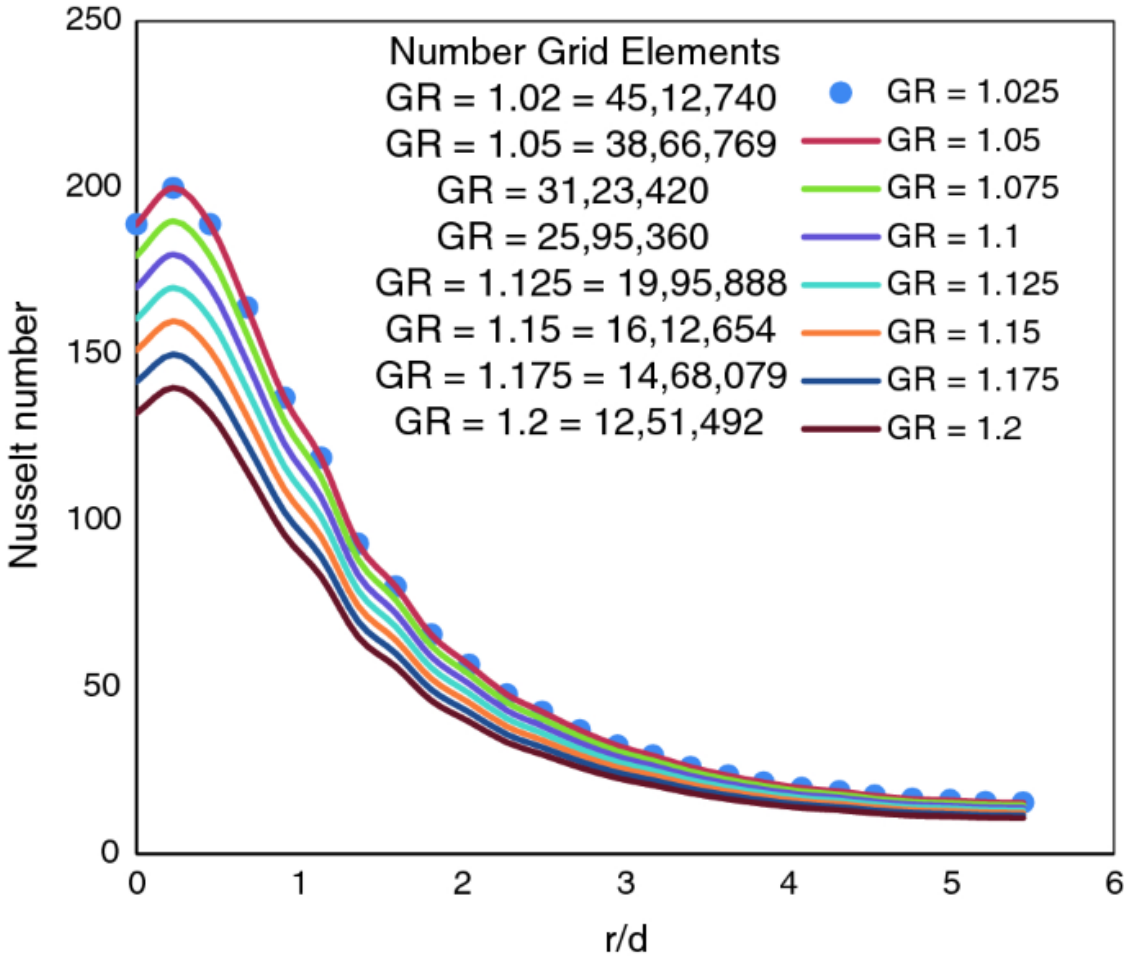

Fig. 2. Local Nusselt number for a different mesh with varying growth rates

Figure 3 represents the current mesh structure with a growth rate of 1.025 along *Z* and *r*. For the growth rate of 1.025, ten mesh cells are observed in a unit millimeter distance (Vertical and horizontal). Hence, the number of elements present horizontally on the surface of the target plate is around 1000, while for nozzle–target spacing of 4, 500 number of elements are present vertically.

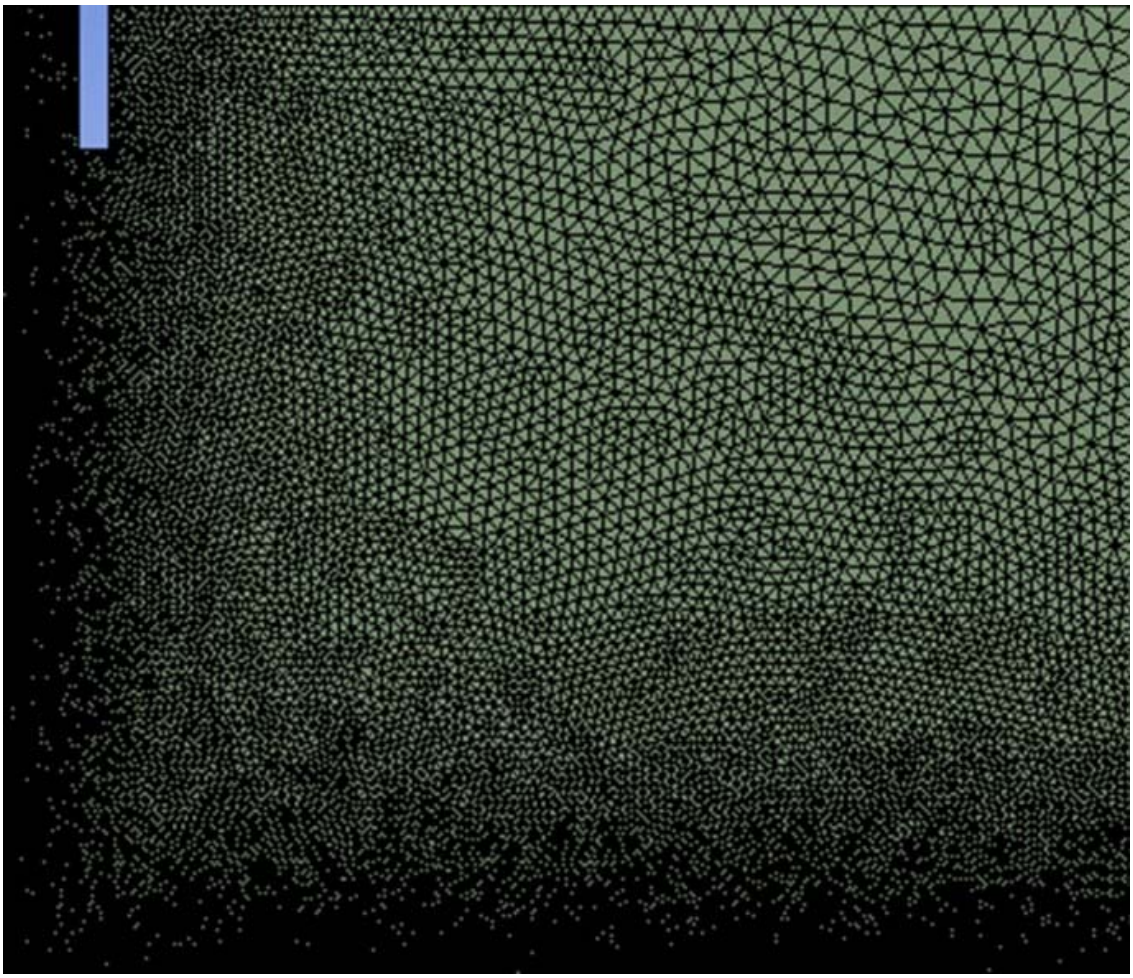

Fig. 3. Hexahedral mesh topology for present geometry with a growth/aspect rate of 1.025

Turbulence modeling and validation

The present study needs to incorporate the heat transfer in the near-wall and far-wall region, for which the proper choice of turbulence model is a must. The heat transfer prediction under jet impingement can be accurately made using a turbulence model that includes both effects (Menter [19]). The use of Shear Stress Transport turbulence for heat transfer determination under air jet is clearly justified by Menter [19]. As seen from the article of Alimohammadi et al. [10], the use of Shear Stress Transport (SST) in combination with Gamma–Theta transition models is quite robust in determining the Nusselt profile for the case of impinging fluid. The validation of the existing computational domain is carried out with the correlation proposed by Katti and Prabhu [2]. These correlations are valid for Z/d=2–8 and quite a wide range of Reynolds numbers (5000–36,000). The turbulence model is also validated against the results of Alimohammadi et al. [7] for Z/d=2–6 and Re=6000, 10,000, and 14,000. The most exciting thing about using the Gamma–Theta transitional model is its ability in capturing the flow behavior due to the adverse pressure difference at the stagnation point and local transition of velocity across the target surface. In addition to this, the onset transition of Reynolds number (velocity gradient) is also captured. The base model, SST, ensures the prediction of flow regimes in the near-wall and far-wall regions (Menter [20]). The art of equation for these turbulence models is well discussed in the latter part of appendix. The

solver uses the continuity (Eq. 1) momentum (Eq. 2) to predict the flow behavior and the universal energy equations to predict the corresponding heat transfer interaction (Srinath [21]).

$$\frac{\partial \rho}{\partial t} + \nabla \left(\rho . \vec{v} \right) = S_{\mathrm{m}} \tag{1}$$

$$\frac{\partial \vec{v}}{\partial t} + \nabla \left(\rho . \vec{v} . \vec{v} \right) = -\Delta p + \Delta \bar{\bar{\tau}} + \rho . \vec{g} + \vec{f} \tag{2}$$

where Δp—change in pressure, $\Delta \bar{\bar{\tau}}$— change in shear stress.

However, to understand the prediction of cooling rate against different turbulence models, a comparative study is carried out at Z/d=4 and Reynolds number of 10,000. As seen, the heat transfer rate prediction using K-Epsilon turbulence model deviates far from accurate results. This is due to the lack of heat transfer rate prediction due to the generation of abnormal turbulence at the target surface. The K-Epsilon turbulence model is generally used to predict flow profile/ heat transfer for a laminar flow in a close conduit. But the use of the K-omega turbulence model gives an accurate profile. However, the magnitude of heat transfer deviates far from real results. This is due to the lack of prediction of turbulence vortices generated due to the adverse pressure gradient due to impingement. Shear stress transport turbulence model carries an additional term responsible for predicting the generation and the termination of local turbulence vortices. Hence, the prediction of heat transfer using this model generates an entirely accurate result. Gamma–Theta turbulence model incorporates the additional turbulence vortices generated due to adverse pressure gradient at stagnation region, onset transition of Reynolds number along the target surface. Hence, the combination of the SST and Gamma–Theta turbulence model gives a quite accurate heat transfer prediction. Figure 4 shows the comparative plot of the Nusselt profile along the target surface for different turbulence models. The comparison is carried at Z/d=4 and Reynolds number of 5000—10,000 since the impinging jet's potential core is just developed before the jet strikes the target surface. (Shadlesky [3]).

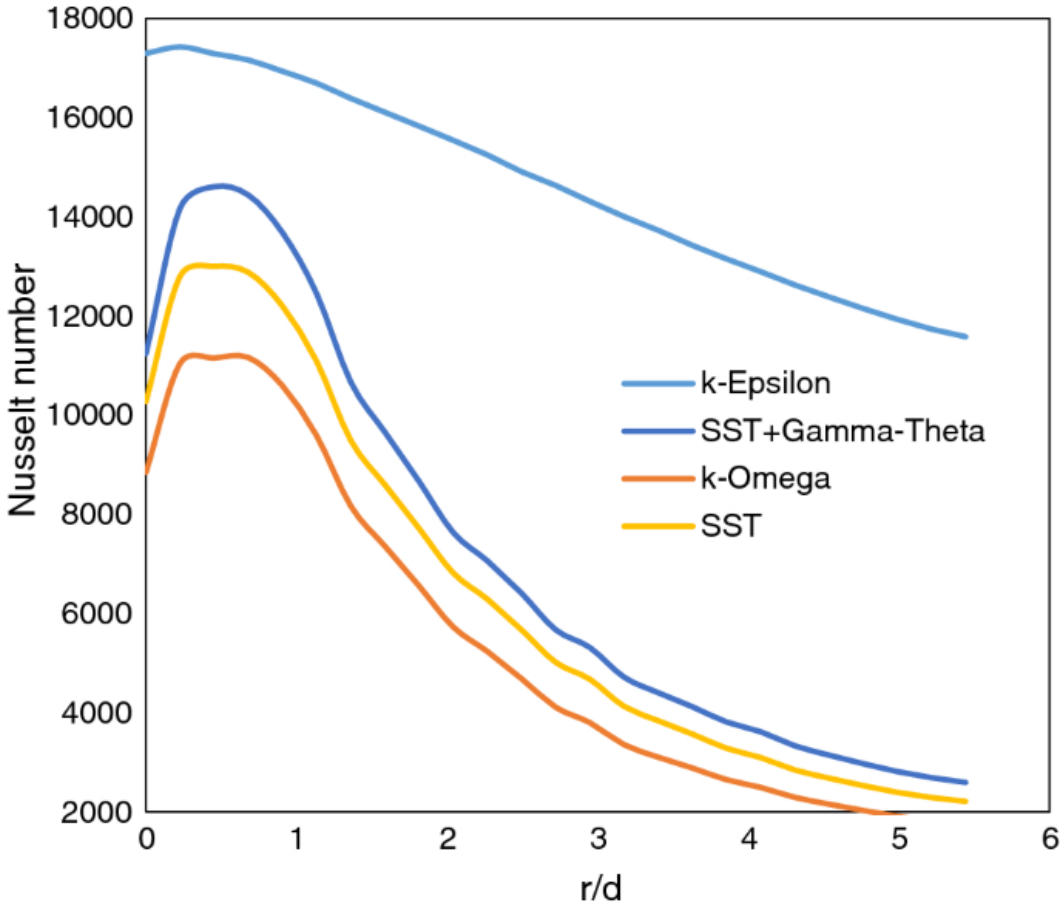

Fig. 4. Nusselt profile of target surface with different turbulence models

The previous results of Katti and Prabhu [2] and Alimohammadi et al. [10] are extracted to validate the current model. The results for local Nusselt numbers from the article of Alimohammadi et al. [10] are taken using an online graph plot digitizer (Universal free access). This is shown in Fig. 5. On the other hand, the present computed results are also compared with that of Katti and Prabhu [2] (this is done with the proposed empirical relation for stagnation region ($0 < r/d < 1$) and transition regions ($1 < r/d < 2.5$)); this is shown in Fig. 6 (a) and (b). The correlation derived by Katti and Prabhu [2] for determining the cooling characteristic (Nusselt profile) is discussed in appendix part. The overall Nusselt number is calculated by averaging the local Nusselt number values at different r/d, while the local Nusselt profiles digitized (Web plot digitizer). This is shown in Eq. (3). It needs to be noted that Eq. (3) is just valid for the present computational domain and is unique. This is only derived for validation purpose. Figure 5 shows the validation of the overall Nusselt number obtained using present computation with the results of Alimohammadi et al. [7]

$$Nu_0 = 0.062Re^{0.7}Z/d^{-0.03} \tag{3}$$

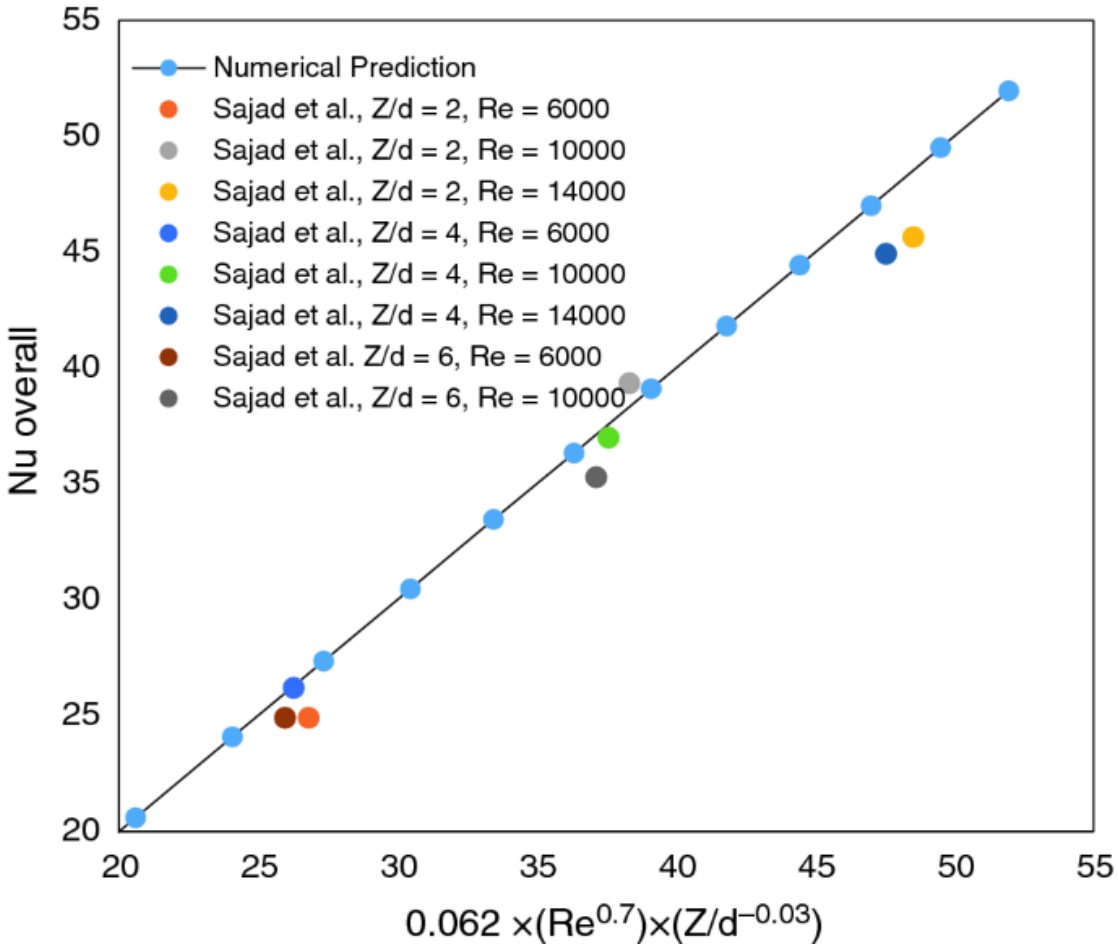

Fig. 5. Validation of present numerical results with that reported by Alimohammadi et al. [7]

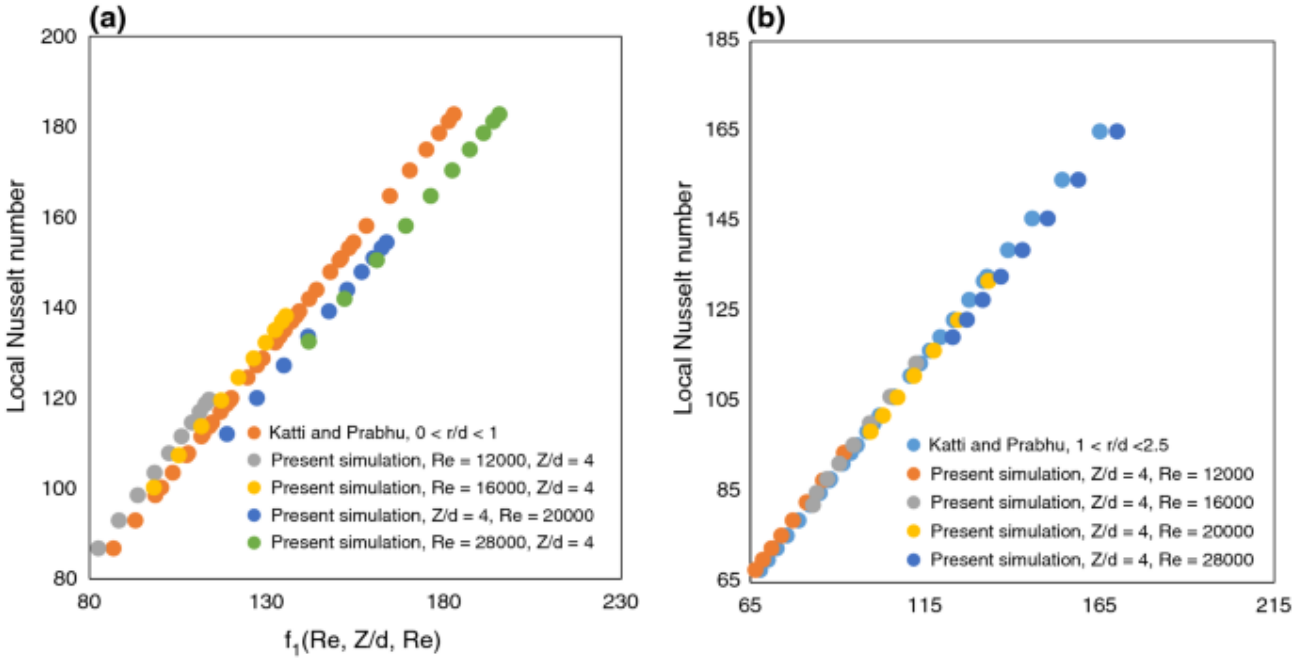

Fig. 6. a and **b** Validation of present numerical results with that reported by Katti and Prabhu [2] for stagnation region ($0 < r/d < 1$) and for transition region ($1 < r/d < 2.5$)

The validation of the present computational grid and turbulence with the results of Katti and Prabhu [2] is shown in Fig. 6 (a) and (b). Katti and Prabhu [2] have defined the correlation for determining the Nusselt number in stagnation region ($0 < r/d < 1$) and transition region ($1 < r/d < 2.5$). The computational geometry was designed as per the dimensions of Katti and Prabhu [2] experimental setup, in which a 0.05-mm-thin stainless steel foil of 80 mm × 160 mm was considered. The jet comes well developed from a 7.35-mm-diameter nozzle and length equal to 83 times the diameter. To avoid the secondary rise in the Nusselt number, according to Siddique et al. [4], the validations are reported for Z/d=4 and Reynolds number of 12,000, 16,000, 20,000 and 28,000. This is shown in Fig. 6 (a) and (b). The correlations, $f_1(Re,Zd,rd)$ and $f_2(Re,Zd,rd)$, are also described in appendix. The approximate percentage error of the present result with Alimohammadi et al. [7] is within ± 7%. However, when compared with the results of Katti and Prabhu [2] for stagnation and transition region, the maximum deviation observed is around ± 12% and the average error is around ± 9%. The error in the present results when compared with Katti and Prabhu [2] is high, since the work of Katti and Prabhu [2] was purely experimental, in which the uncertainty specified was around ± 15%.

Nusselt profile for different ramp input boundary condition

Nusselt profiles are evaluated for different ramp inputs, heat flux boundary condition, Reynolds number, and Z/d. According to Siddique et al. [4, Siddique et al. [12], the secondary peaks start occurring at Rez=176,400, so considering Z/d=6, the maximum Reynolds number turns out to be around 30,000. Hence, the upper limit of present computation must not exceed the nozzle – target spacing of 6 and Reynolds number of 30,000. The least value of Z/d observed as per the experiments of Katti, and Prabhu [2] is 1, since, below this value, the phenomenon of heat transfer is not usual and is beyond the capability of the current turbulence model (Siddique et al. [4, Siddique Mohd et al. [19, Siddique et al. [22]), whereas the least Reynolds number can be chosen to just above tot the start of the turbulent region (Re = 30,000). Hence, computation shall be carried out for different slopes of ramp input heat flux boundary condition considering Z/d=4 and Re=5000. An average slope shall then be decided to predict Nusselt profile behavior for different Reynolds numbers (3000–30,000) by keeping Z/d=4. The variation in the Nusselt profile for an average slope of ramp input heat flux and Reynolds numbers of 5000 shall be observed for different Z/d (1–6). The ramp heat flux input boundary is given in Eq. (4), where m indicates the slope and $Q0$ represents the means of constant heat flux magnitude (Wm^{-2}). The value of this constant heat flux chosen is 92.5 KWm^{-2} (Yunus A Cenjel [14]). This magnitude of flux just sufficient for producing a bulk mean temperature rise of $100C$ for a flow occurring in a pipe of unit meter length (Yunus A Cenjel [14]). However, the Nusselt number magnitude remains independent of heat flux input, as Katti and Prabhu [2]. The variable x in Eq. 4 indicates the local radial location.

$$Q = Q_0 \times mx \tag{4}$$

Nusselt profile for different slope of ramp input heat flux boundary condition with constant Reynolds numbers and Z/d

Figure 7 shows the Nusselt profile at different slopes of ramp heat flux with constant Reynolds numbers of 5000 and Z/d=4. The slope of ramp heat input is varied from 0.1, 0.2, 0.3, 0.4, 0.5, 0.6, 0.7, 0.8, 0.9 up to 1. The heat dissipation was observed to better at lower

values of the slope of ramp heat input (Fig. 7). As shown in Fig. 7, with an increase in the slope, the Nusselt profile shows decrement. The magnitude of local Nusselt number for the impinging parameters of Z/d=4 and Reynolds number of 5000 increases with a decrease in the slope (m). The increase in the slope represents the increase in the magnitude of heat flux input. However, the Nusselt profile distribution for varying/constant heat flux input boundary conditions in a non-uniform manner depends on the area under the curve (Heat flux input V/s radial distance). Figure 8 shows the velocity distribution under the nominal impinging parameter (Z/d = 4, Reynolds number = 5000), for the 0.1, 0.5 and 1. The velocity distribution for the slope of 0.1 gives the scattered impingement spots, which are generated from the upper skin of the stagnation region. Due to such impingement spots, a higher cooling rate is observed for the varying heat flux boundary condition's lower slope. Hence, the higher magnitude of the Nusselt number is observed for the same.

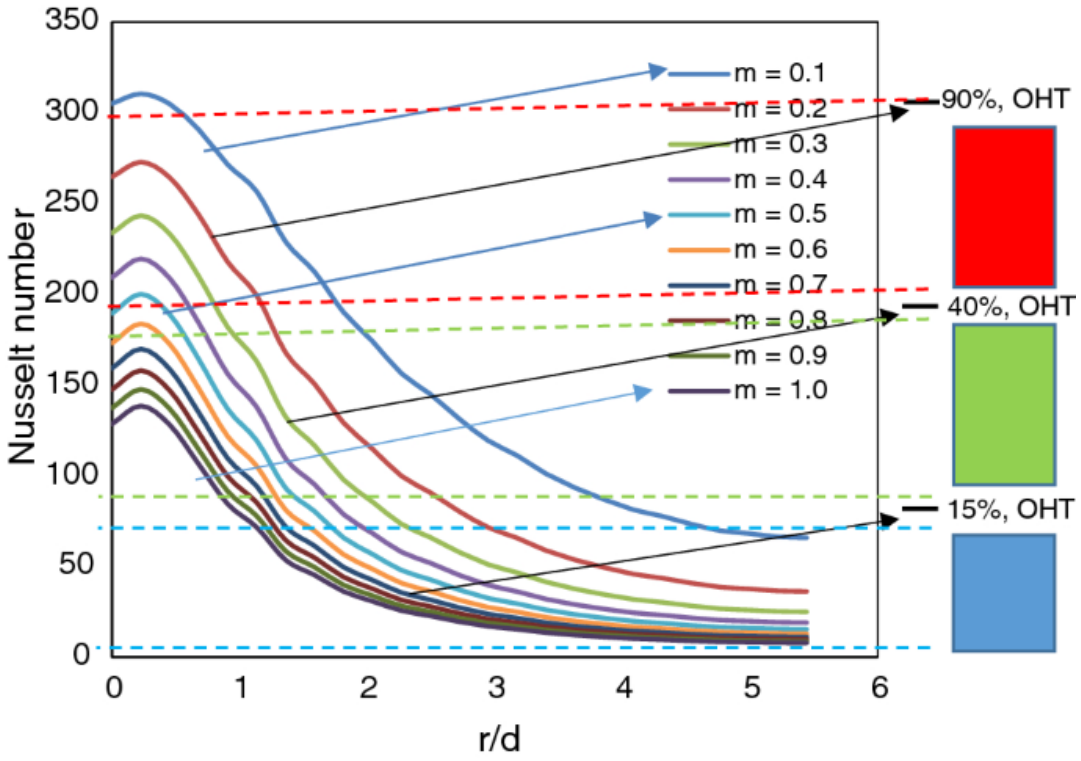

Fig. 7. Nusselt profile at the different slope of ramp input with constant Reynolds numbers and constant Z/d (OHT—Overall Heat Transfer)

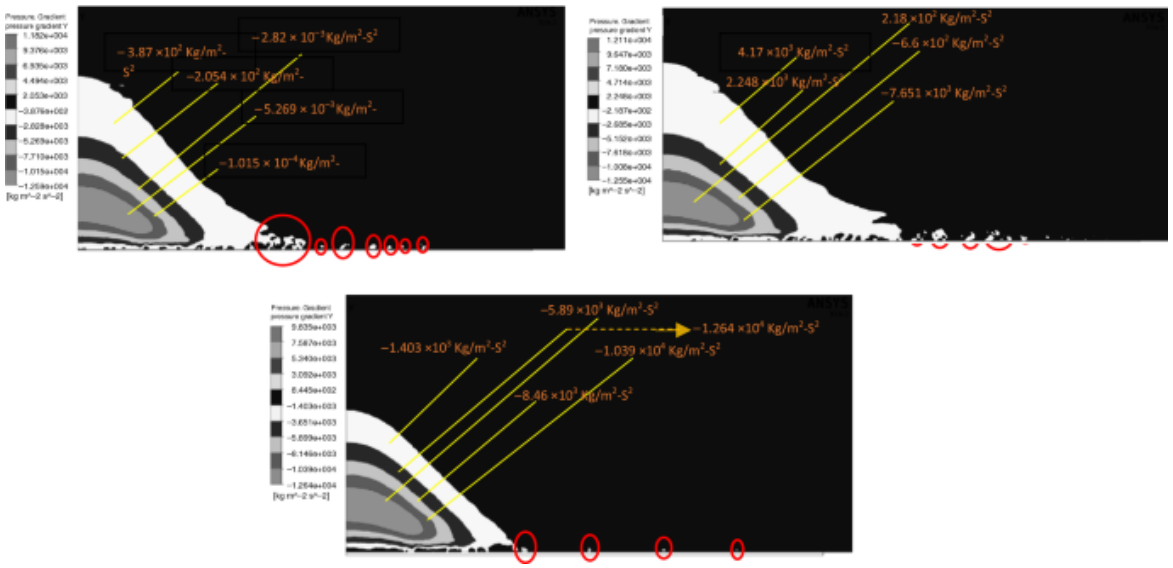

Fig. 8. Velocity contours for stagnation, transition, and far wall region under different slope (m=0.1, 0.5 and 1) of varying heat flux boundary condition

Nusselt profile for different Reynolds number and nozzle–target spacing with unit slope

Figure 9 (a) shows the Nusselt profile at different Reynolds numbers with unit slope and constant Z/d of 4. In this case, the Reynolds number is varied 2000, 4000, 6000, 8000, 10,000, 12,000, 14,000, 16,000, 18,000 and 20,000. Unit slope ramp heat input is applied with Z/d=4. An increase in Reynolds number conveys the increase in Nusselt number magnitude and shifting the Nusselt profile toward a positive y scale. At the higher velocity, the heat is carried away quickly, and thus, forced convection renders a better heat transfer coefficient. The varying heat flux boundary condition slope is chosen as unity to avoid the heat flux boundary condition. Hence, Fig. 9(a) shows the Nusselt profile variation only due to variation in Reynolds number. Figure 9 (b) shows the Nusselt profile at different Z/d with unit slope and constant Reynolds number of 5000. Z/d is varied from 1, 2, 3, 4, 5, 6, 7, 8, 9 up to 10. As the nozzle distance from the target surface is increased, the local Nusselt magnitude reduces (Fig. 9(b)). However, this is not valid for Z/d=1, 2, and 3, since the impinging momentum of air in this region of Z/d does not allow the potential core to develop; hence there is an occurrence of peaks (Siddique et al. [4]). However, the potential core at Reynolds number of 5000 is well developed for the rest values of Z/d. Hence the smooth profile of the Nusselt number is observed. Above the value of Z/d=10, the Nusselt number doesn't show any augmentation (Increment/Decrement); hence the computations are done only up to Z/d =10. The occurrence of secondary peak in the Nusselt profile in Fig. 9 (a) and (b) Nusselt at different Reynolds number with unit slope and constant Z/d Fig. 9(a) and (b), is due to underdevelopment of the potential core of the impinging jet.

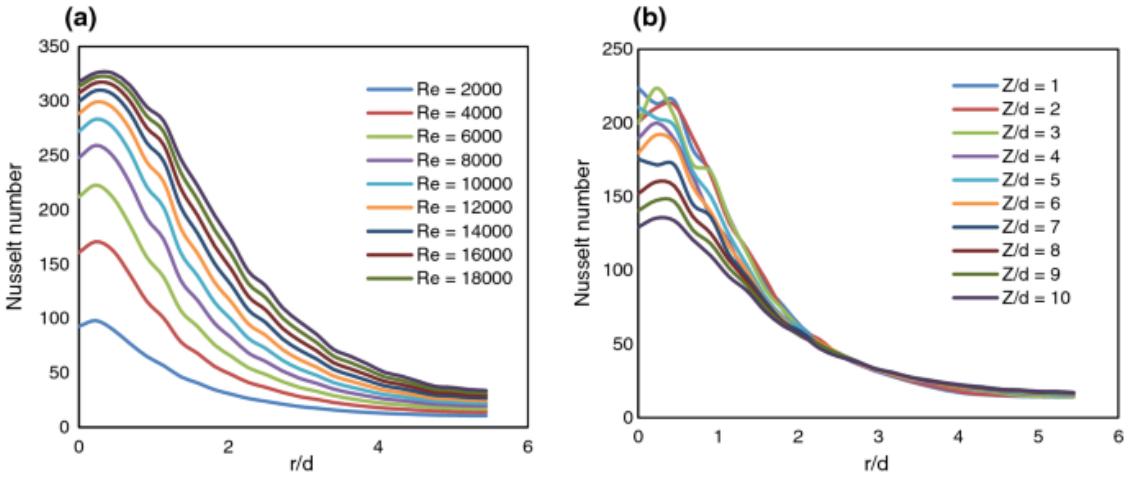

Fig. 9. a and **b** Nusselt at different Reynolds number with unit slope and constant Z/d Nusselt profile at different Z/d with unit slope and constant Reynolds number

The secondary peak in the Nusselt profile is due to the underdevelopment of potential core and high penetrating momentum. To see the effect of Reynolds number and Z/d, the author takes the initiative to plot the velocity contour for the nondimensional term $(C = \frac{Re}{Z/d})$. The secondary peak in the Nusselt profile is due to transition skin, just beside the stagnation region. Figure 10 justifies the same.

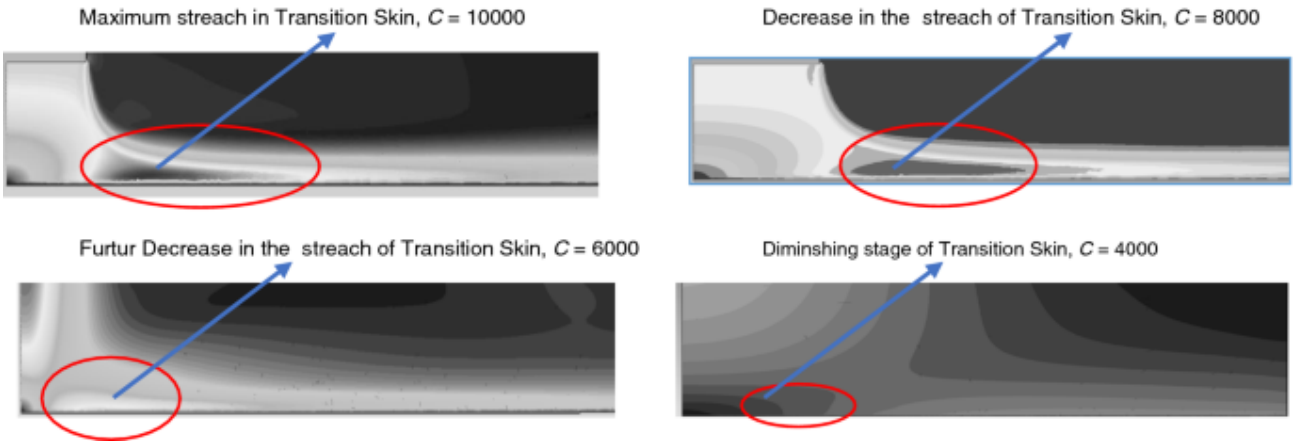

Fig. 10. Velocity Contours for C=10,000, 8000, 6000 and 4000

Semi-empirical relations representing Nusselt profile

While deriving the Nusselt number magnitude as a function of Reynolds number, Z/d

, and slope of ramp input heat flux, it was observed that a single unique empirical relation doesn't render a good regression coefficient. Also, Katti and Prabhu [2] have derived the correlation relation for Nusselt number separately for three different regions ($0 < r/d < 1$, $1 < r/d < 2.5$ and $r/d > 2.5$). In the present case the Nusselt number empirical relation is proposed for stagnation region ($0 < r/d < 1$), transition field ($1 < r/d < 2.5$) and wall jet field ($r/d > 2.5$). Table 1 shows the corresponding correlation for every individual regions.

Figure 11 shows the best fit line for all the readings plotted against the respective semi-empirical relation with an error bar of ±20%.

Table 1 Proposed Correlation for local Nusselt number different regions

r/d	Function	Semi-empirical relation
$0 < r/d < 1$	$F_1\left(Re, \frac{Z}{d}, m, \frac{r}{d}\right)$	$Nu = 0.22 \times (Re)^{0.75}\left(\frac{z}{d}\right)^{-0.01}(m)^{-0.32}\left(\frac{r}{d}\right)^{-0.07}$
$1 < \frac{r}{d} < 2.5$	$F_2\left(Re, \frac{Z}{d}, m, \frac{r}{d}\right)$	$Nu = 0.016 \times (Re)^{0.97}\left(\frac{Z}{d}\right)^{0.3}(m)^{-0.52}\left(\frac{r}{d}\right)^{-1.26}$
$\frac{r}{d} > 2.5$	$F_3\left(Re, \frac{Z}{d}, m, \frac{r}{d}\right)$	$Nu = 0.117 \times (Re)^{0.72}\left(\frac{Z}{d}\right)^{0.23}(m)^{-0.635}\left(\frac{r}{d}\right)^{-1.17}$

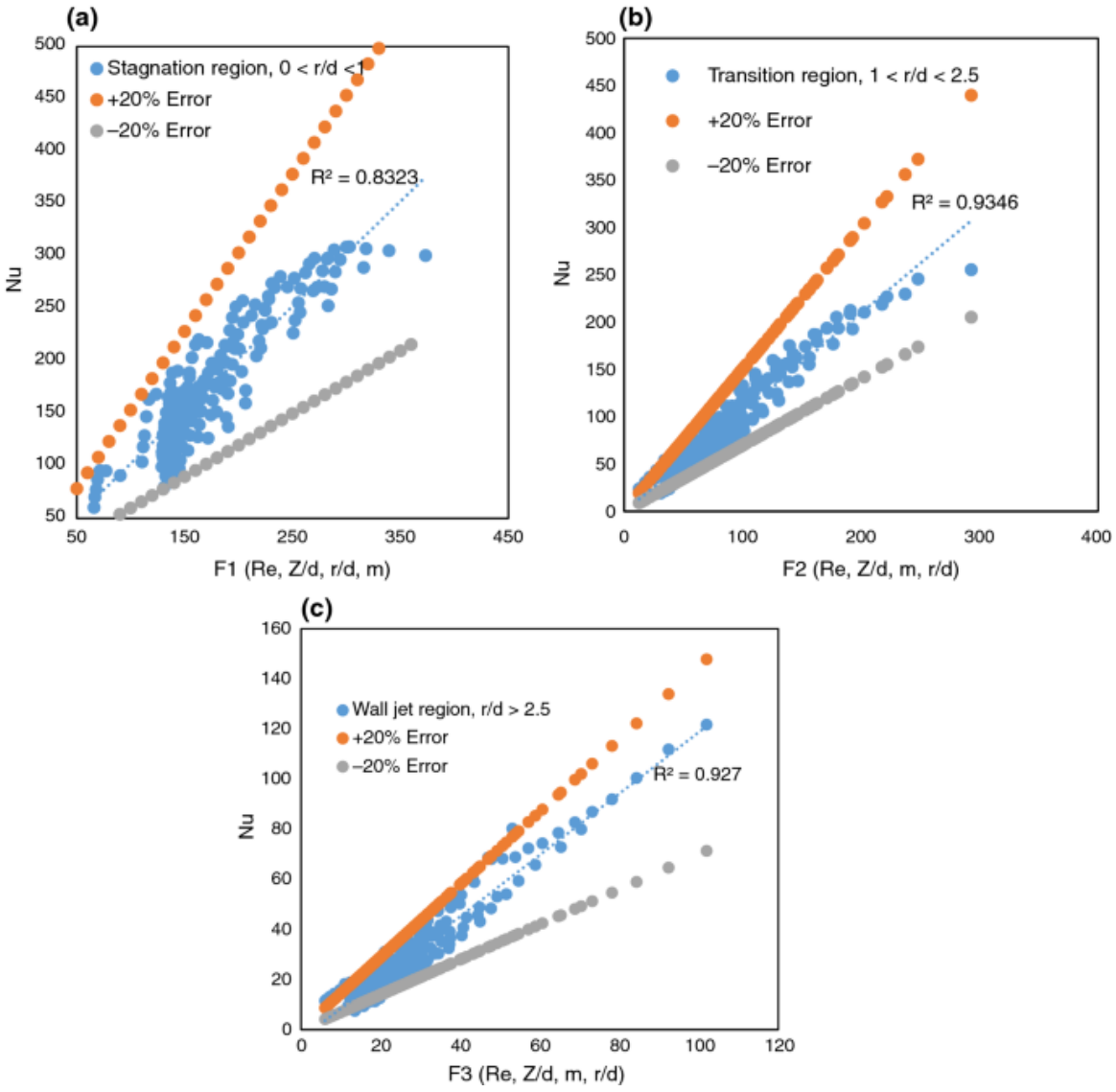

Fig. 11. a, b, and **c** Validation of F_1(Re, Z/d, r/d, m), F_2(Re, Z/d, r/d, m), and F_3(Re, Z/d, r/d, m) with local Nusselt numbers, respectively

Conclusions

The numerical methodology reported in the present, using SST and Gamma–Theta transition model, proves to predict the Nusselt profile's value quite accurately. The turbulence phenomenon of intermediacy, flow separation, local velocity gradient, and the transition is successfully captured. The Nusselt profile's (local Nusselt number) is significantly affected by the heat flux profile (m). The proposed empirical relation's exponents carry a negative power of –0.32 to –0.635, which justifies the inverse dependency on the slope of varying heat flux boundary conditions. Also, it is seen that the Nusselt number is the least affected by the nozzle–target spacing in the stagnation region. This is due to the impinging jet's penetrating momentum dominating the velocity gradient's development. However, after the stagnation region, the velocity gradient development over the target surface dominates. The effect of impingement (Re) produces almost a similar impact on all three vital areas of the target surface. This is quite unusual when one compares the empirical relation for local Nusselt number under constant heat flux boundary conditions. The dependency of the nozzle–target spacing carries a more significant impact under such boundary conditions due to the later development of a thermal boundary layer. This is because of the varying heat flux boundary condition. The same can be justified through a secondary peak in the Nusselt profile near the stagnation region.

Future scope

A fascinating further scope in the present article lies in determining the Nusselt profile under a constant temperature boundary condition. A comparison between the profile heat flux for steady heat flux boundary conditions and profile heat flux for continuous temperature boundary conditions may better understand the Nusselt profile for these two boundary conditions. The work can also be extended in developing some modified non-dimensional number, which represents the slope of the heat flux profile in the present article.

Acknowledgement

The articles' authors are very pleased with the co-operation, guidelines, and computational facility provided by the Center of High-Performance Computing (CHPC), Cape Town, South Africa.

References

1. Pamadi B, Belov I. A note on the heat transfer characteristics of circular impinging jet. Int J Heat Mass Transf. 1980;23(6):783–7.
2. Katti V, Prabhu S. Experimental study and theoretical analysis of local heat transfer distribution between smooth flat surface and impinging air jet from a circular straight pipe nozzle. Int J Heat Mass Transf. 2008;51(17–18):4480–95.
3. Shadlesky P. Stagnation point heat transfer for jet impingement to a plane surface. AIAA J. 1983;21(8):1214–5.
4. Siddique U, Ansari E, Khan SA, Patil R. Numerical Investigation of Secondary Peaks in Nusselt Profile Under Water Jet Impingement. J Thermophys Heat Transfer. 2020;34(2):421–8.
5. Jambunathan K, Lai E, Moss M, Button B. A review of heat transfer data for single circular jet impingement. Int J Heat Fluid Flow. 1992;13(2):106–15.

6. Mohanty A, Tawfek A. Heat transfer due to a round jet impinging normal to a flat surface. Int J Heat Mass Transf. 1993;36(6):1639–47.
7. Alimohammadi S, Murray D, Persoons T. Experimental validation of a CFD methodology for transitional flow heat transfer characteristics of a steady impinging jet. J Heat Transf. 2014;136:091703.
8. Alimohammadi, S., *A Validated Computational Fluid Dynamics Methodology for Characterisation of Fluid Flow & Heat Transfer in Unsteady Jets*. 2016, Trinity College Dublin.
9. Sailor DJ, Rohli DJ, Fu Q. Effect of variable duty cycle flow pulsations on heat transfer enhancement for an impinging air jet. Int J Heat Fluid Flow. 1999;20(6):574–80.
10. Alimohammadi, S., D.B. Murray, and T. Persoons, *Experimental validation of a computational fluid dynamics methodology for transitional flow heat transfer characteristics of a steady impinging jet.* Journal of Heat Transfer, 2014. **136**(9).
11. Sagot B, Antonini G, Christgen A, Buron F. Jet impingement heat transfer on a flat plate at a constant wall temperature. Int J Therm Sci. 2008;47(12):1610–9.
12. Siddique UM, Bhise GA, Gulhane NP. On numerical investigation of local Nusselt distribution between flat surface and impinging air jet from straight circular nozzle and power law correlations generation. Heat Transf Asian Res. 2018;47(1):126–49.
13. Ekkad SV, Kontrovitz D. Jet impingement heat transfer on dimpled target surfaces. Int J Heat Fluid Flow. 2002;23(1):22–8.
14. Yunus A Cenjel, A.J.G., <*Heat_and_Mass_Transfer_Fundamentals_and.pdf*>.
15. Zuckerman N, Lior N. Jet impingement heat transfer: physics, correlations, and numerical modeling. Adv Heat Transf. 2006;39:565–631.
16. Umair SM, Gulhane NP. On numerical investigation of nonuniformity in cooling characteristic for different materials of target surfaces being exposed to impingement of air jet. Int J Model Simul Sci Comput. 2017;8(03):1750024.
17. Behnia M, Parneix S, Shabany Y, Durbin P. Numerical study of turbulent heat transfer in confined and unconfined impinging jets. Int J Heat Fluid Flow. 1999;20(1):1–9.
18. Ricou FP, Spalding D. Measurements of entrainment by axisymmetrical turbulent jets. J Fluid Mech. 1961;11(1):21–32.
19. Siddique Mohd U, Ansari E, Khan SA, Gulhane NP, Patil R. Numerical Investigation of Nondimensional Constant and Empirical Relation Representing Nusselt Profile Nonuniformity. J Thermophys Heat Transf. 2020;34(1):215–29.
20. Menter FR. Influence of freestream values on k-omega turbulence model predictions. AIAA J. 1992;30(6):1657–9.
21. Srinath, S., *Modeling and prediction of near wall turbulent flows*. 2017.
22. Siddique, U., E. Ansari, S.A. Khan, and R. Patil, *Numerical Investigation of Semi-Empirical Relation Representing Nusselt Number Under Waterjet Impingement.* J Thermophys Heat Transf, 2020.
23. Sparrow EM, Gorman JM, Abraham JP, Minkowycz W. Validation of turbulence models for numerical simulation of fluid flow and convective heat transfer. In: Advances in Heat Transfer. London: Elsevier; 2017. p. 1–35.

Appendix

Turbulence Model, Menter [20], Sparrow et al. [23], and Srinath [21]

K-Epsilon model

$$\mu_{\text{eff}} = \mu_{\text{t}} + \mu$$

$$\mu_{\text{t}} = \frac{C\rho K^2}{\epsilon}$$

K-Equation

$$\frac{\partial(\rho K)}{\partial t} + \frac{\partial(\rho U_{\text{j}} K)}{\partial x_{\text{j}}} = \frac{\partial}{\partial x_{\text{j}}}\left\{\left[\mu + \frac{\mu_{\text{t}}}{\sigma_{\text{k}}}\right]\frac{\partial K}{\partial x_{\text{j}}}\right\} + P_{\text{k}} - \rho\varepsilon + P_{\text{kb}}$$

$$P_{\text{kb}} - Bouyant\ term = \mu_{\text{t}}\left[\frac{\partial U_{\text{j}}}{\partial x_{\text{j}}} + \frac{\partial U_{\text{j}}}{\partial x_j}\right] - \frac{2}{3}\frac{\partial U}{\partial x}\left[3\mu_t\frac{\partial U_k}{\partial x_k} + \rho K\right]$$

Epsilon equation

$$\frac{\partial(\rho\epsilon)}{\partial t} + \frac{\partial(\rho U_j \varepsilon)}{\partial x_j} = \frac{\partial}{\partial x_j}\left\{\left[\mu + \frac{\mu_t}{\sigma_\varepsilon}\right]\frac{\partial \varepsilon}{\partial x_j}\right\} + \frac{\varepsilon}{K}$$
$$\left[C_{\varepsilon 1}P_k - C_{\varepsilon 2}P\varepsilon + C_{\varepsilon 1}P_{\varepsilon b}\right]$$

K-Omega model,

Near-wall treatment is good

$$\mu_{\text{t}} = \frac{\rho K}{\omega}$$

K-equation

$$\frac{\partial(\rho K)}{\partial t} + \frac{\partial(\rho U_{\text{j}} K)}{\partial x_{\text{j}}} = \frac{\partial}{\partial x_{\text{j}}}\left\{\left[\mu + \frac{\mu_{\text{t}}}{\sigma_{\text{k}}}\right]\frac{\partial K}{\partial x_{\text{j}}}\right\} + P_{\text{k}} - \beta\rho K\omega + P_{\text{kb}}$$

Turbulence production term is modified.

Omega equation

$$\frac{\partial(\rho\omega)}{\partial t} + \frac{\partial(\rho U_{\text{j}}\omega)}{\partial x_{\text{j}}} = \frac{\partial}{\partial x_{\text{j}}}\left\{\left[\mu + \frac{\mu_{\text{t}}}{\sigma_{\omega}}\right]\frac{\partial\omega}{\partial x_{\text{j}}}\right\} + \frac{\alpha\omega}{K}P_{\text{k}} - \beta\rho K\omega^2 + P_{\omega\text{b}}$$

Shear stress transport model

$$\vartheta_{\text{t}} = \frac{a_1 K}{max(a_1, \omega, SF_2)}$$

S—Invariant strain rate.

Takes combination effect of K-Epsilon and K-omega.

Behaves as K- omega in the near-wall region and K-Epsilon in the far-wall region

$$\frac{\partial(\rho K)}{\partial t}+\frac{\partial\left(\rho U_{\mathrm{j}} K\right)}{\partial x_{\mathrm{j}}}=\frac{\partial}{\partial x_{\mathrm{j}}}\left\{\left[\mu+\sigma_{\mathrm{k}} \mu_{\mathrm{t}}\right] \frac{\partial K}{\partial x_{\mathrm{j}}}\right\}+P_{\mathrm{k}}-\beta \rho K \omega$$

It doesn't consider the buoyant force.

Turbulence production term is modified

$$\frac{\partial(\rho \omega)}{\partial t}+\frac{\partial\left(\rho U_{\mathrm{j}} \omega\right)}{\partial x_{\mathrm{j}}}=\frac{\partial}{\partial x_{\mathrm{j}}}\left\{\left[\mu+\frac{\mu_{\mathrm{t}}}{\sigma_{\omega}}\right] \frac{\partial \omega}{\partial x_{\mathrm{j}}}\right\}+2\left(1-F_{\mathrm{t}}\right) \rho \frac{1}{\rho_{\omega 2}} \frac{\partial K}{\partial x_{\mathrm{j}}} \frac{\partial \omega}{\partial x_{\mathrm{j}}}+\alpha_3 \frac{\omega}{K} P_{\mathrm{k}}-\beta \omega \rho^2$$

F_t—Blend factor which switches in near-wall and far-wall region.

Gamma model

$$Re_{\mathrm{v}}=\frac{\rho y^2 S}{\mu}$$

$y^2 S-$ Degree of disturbance

$\frac{\rho}{\mu}-$ Damping term

Re_v- Vorticity based Reynolds number.

$$P_\gamma=F_{\text{length}} C_1 \rho S\left[\gamma F_{\text{onset}}\right]^{0.5}(1-C\gamma)$$

$F_{\text{length}}-$ Controls the length of intermediancy

$F_{\text{length}}=$ Empirical correlation in terms of $Re_{\theta t}$

$$Re_{\theta \mathrm{t}}=\frac{\rho V \theta}{\mu}$$

$$F_{\text{onset}} = \frac{Re_{\text{v}}}{2.193 Re_{\theta c}}$$

$Re_{\theta c}$ = Critical Reynold number where intermediancy starts

$$\frac{\partial(\rho\gamma)}{\partial t} + \frac{\partial(\rho U_{\text{j}}\gamma)}{\partial x_{\text{j}}} = \frac{\partial}{\partial x_{\text{j}}}\left\{\left[\mu + \frac{\mu_{\text{t}}}{\rho}\right]\frac{\partial\gamma}{\partial x_{\text{j}}}\right\} + P_{\text{k}} - E_{\gamma}$$

E_{γ} – Defines the destruction of intermediancy and relaminarisation stage

$$E_{\gamma} = C\rho\gamma F_{\text{turb}}(C\gamma - 1)$$

Magnitude of vorticity (No. of recirculation zone)

$$Re_{\text{v}} = \frac{\rho V}{\mu}$$

Theta model

$$\frac{\partial(\rho Re_{\theta t})}{\partial t} + \frac{\partial(\rho U Re_{\theta t})}{\partial x_{\text{j}}} = \frac{\partial}{\partial x_{\text{j}}}\left\{\sigma_{\theta t}(\mu + \mu_{\text{t}})\frac{\partial Re_{0}}{\partial x_{\text{j}}}\right\} + P_{\theta t}$$

$\frac{\partial(\rho Re_{\theta t})}{\partial t}$ - Considers onset transition of Reynolds number

Controls the arena of intermediacy

$P_{\theta t}$ – Controls the flow in boundary layerr, beyoung it it is non active

$Re_{\theta t}$ = Onset Momentum Reynolds number

$$P_{\theta t} = C_{\theta t}\frac{\rho}{t}(Re_{\theta t} - Re *_{\theta t})(1 - F_{\theta t})$$

$Re *_{\theta t}$ – Fixedvalue = Free stream Reynolds number.

$t = \frac{500\mu}{\rho\mu^2}$. only for the non-dimensional purpose

$F_{\theta t}$ - Varies in vertical direction, 0.2, 0.3, 0.8 and outside the boundary laye value is 1

Correlations for local Nusselt value by Katti and Prabhu [2]

Regions	Empirical relations
$0 < r/d < 1$	$Nu = a_1 Re^{0.5} Pr^{0.33} \left(\frac{Z}{d}\right)^{-0.11}$
$1 < r/d < 2.5$	$Nu = 0.263 Re^{0.6188} \left(\frac{Z}{d}\right)^{-0.08} \left(\frac{r}{d}\right)^{-0.307}, Z/d \leq 3$
	$Nu = 0.195 Re^{0.66} \left(\frac{Z}{d}\right)^{-0.08} \left(\frac{r}{d}\right)^{-0.3702}, Z/d \geq 4$
$r/d > 2.5$	$Nu = 0.0436 ERe^{0.8} Pr^{0.33} \left(\frac{Z}{d}\right)^{0.097}$